International Journal of Applied Power Engineering (IJAPE)
Vol. 15, No. 1, March 2026, pp. 211~227
ISSN: 2252-8792, DOI: 10.11591/ijape.v15.i1.pp211-227

Modeling H_2-enriched dual fuel engine performance and emissions

Jayagopal Narayanan[1], Y. V. V. Satyanarayana Murthy[2], Sandeep Kumar[1], Talari Surendra[3], Ram Mohan Rao Madaka[3]
[1]Department of Marine Engineering, Indian Maritime University, Chennai, India
[2]Department of Marine Engineering, School of Marine Engineering and Technology, Indian Maritime University, Chennai, India
[3]GITAM (Deemed to be University), Visakhapatnam, India

Article Info

Article history:

Received Jul 11, 2025
Revised Oct 30, 2025
Accepted Nov 28, 2025

Keywords:

Dual fuel engine
H_2 enrichment
NOx neutral
Performance
Random forest
Response surface methodology

ABSTRACT

This study utilizes a validated GT-Power simulation model to evaluate hydrogen (H_2) enrichment effects on the performance and emissions of a four-cylinder, 86 kW dual-fuel diesel engine. The primary goal is identifying operating strategies that enhance efficiency while maintaining nitrogen oxide (NO_x) emissions at or below baseline levels, termed "NO_x neutral" operation. The methodology involves adjusting engine load between 2 and 16 bar brake mean effective pressure (BMEP) and varying H_2 energy substitution from 10% to 70% at 1500 rpm. To analyse complex non-linear relationships, this research employed response surface methodology (RSM) and a random forest (RF) machine learning algorithm. Results indicate optimal H_2 substitution lies in the 20–30% range, yielding a 2–3% improvement in brake thermal efficiency (BTE) and a significant decrease in brake specific fuel consumption (BSFC) from 200–220 g/kWh to 160–180 g/kWh. While CO_2, HC, and CO emissions decreased, NO_x remained stable only up to 25% substitution, increasing sharply thereafter. Consequently, H_2 energy contribution should be limited to 25% to effectively control NO_x. The combined use of simulation with RSM and RF models proves an efficient, accurate method for engine analysis, minimizing extensive physical testing requirements.

Corresponding Author:

Y. V. V. Satyanarayana Murthy
Department of Marine Engineering, School of Marine Engineering and Technology
Indian Maritime University
Chennai 600019, Tamil Nadu, India
Email: yvvsnmurthy@imu.ac.in

1. INTRODUCTION

The issue of global warming, driven by fossil fuel emissions, is accelerating the search for clean energy alternatives. Hydrogen (H_2) is emerging as a promising carbon-free fuel [1]. Using H_2 in existing internal combustion engines offers a practical way to decarbonize transportation and reduce its carbon footprint [2], [3]. However, employing pure H_2 in engines presents difficulties due to complex combustion processes and increased NO_x emissions [4]. Modifying diesel engines to operate in a dual-fuel setup, where H_2 is the primary fuel and diesel is used for ignition, is a crucial step towards lowering these emissions [5].

The main challenge in converting existing engines to H_2-diesel dual-fuel is controlling NO_x emissions to levels comparable to those of pure diesel, ensuring compliance with regulatory standards. Most in-production engines rely on a traditional mechanical diesel fuel injection system, which has a fixed, single-pulse injection and timing. This inflexibility restricts the ability to optimize injection strategies or integrate additional exhaust gas treatment systems (EGT). Furthermore, operational limits with H_2 are also a constraint, with one

study suggesting that H_2 substitution should be limited to 35% for loads below 50% and 15% for loads above 50% to ensure stable and efficient operation [6]. To optimize dual fuel performance, various control strategies are employed. Injection strategies of both H_2 and diesel are tailored to influence combustion characteristics [7], [8]. Although research on H_2-diesel dual-fuel engines is expanding, a significant gap remains in achieving performance and emission advantages, especially while keeping NO_x emissions neutral. This challenge is particularly relevant for in-production engines, which lack the flexibility of pilot fuel injection and the use of EGT. The majority of published research has focused on single-cylinder engines operating at low loads (brake mean effective pressure (BMEP) under 10 bar) [9], [10]. Consequently, there is a considerable shortage of information on achieving NO_x neutral performance in multi-cylinder, turbocharged in-production engines, particularly at high loads and with increased H_2 energy substitution rates where controlling NO_x poses the greatest challenge [11], [12].

To address this gap, this study utilizes a validated simulation model created with Gamma Technologies (GT-Power). To manage the intricate, non-linear connections between engine parameters and outputs, this research applies two effective techniques: response surface methodology (RSM) for engine optimization [13]-[15], and the random forest (RF) machine learning algorithm for reliable data-driven predictions [16]-[18]. The RF machine learning technique acts as a "virtual engine," allowing for a more efficient exploration of complex trade-offs and precise identification of optimal operating conditions than traditional physical experiments. This study assesses engine performance over a broad spectrum of loads, from 2 to 16 bar BMEP, with H_2 energy substitution ranging from 10% to 70%. The goal is to determine the best operating strategies that enhance efficiency while complying with emission regulations. For this study, H_2 is inducted into the intake system through a port fuel injection (PFI) technique at varying flow rates to ensure a homogeneous air-fuel mixture.

The novelty of this work is a two-fold contribution: A statistical and machine learning methodology was applied to validated simulation data to create a "virtual engine." This approach was extended to a broad range of BMEP for dual-fuel engines, up to 16 bars, and enabled a strategy that increased H_2 substitution without altering the engine's architecture (specifically, the mechanical single-pulse diesel fuel injection system). This work also resulted in a dual-fuel system calibration strategy that maintained the engine-out NO_x level while reducing all carbon-based emissions (CO, CO_2, and HC) and improving thermal efficiency by 2.5%. The subsequent sections of this paper detail the methodology, including the simulation software and sub-models used, the validation process, the application of machine learning, and the results of optimizing H_2 substitution across various BMEP levels.

2. METHOD

In order derive the maximum H_2 substitution and extend the BMEP range of the engine entirely through experiment is time consuming and involve lot of cost. Simulation models validated using experimental data are therefore used for engine calibration optimisation to reduce the time and money involved in this process. Machine learning techniques are able to create virtual engine models which can be further reused for optimisation (increase thermal efficiency and reduce emission).

2.1. Numerical analysis

A one-dimensional engine model was developed in GT-power to replicate the combustion process of a H_2-diesel dual-fuel engine. The simulation employs an advanced calibration procedure that modifies two predictive combustion models: DI-Pulse for the diesel pilot injection and SITurb for the premixed H_2 charge. The simulation schematic layout of the GT-Power model shown in the Figure 1. The calibration process initiates with the cylinder pressure object attribute (CPOA) tool [19], which evaluates experimental in-cylinder pressure data to derive a target net heat release rate (HRR) curve. This curve signifies the total energy released by both fuels. The objective of the calibration is to iteratively adjust the DI-Pulse and SITurb models until their combined HRR output aligns with this target curve. Initially, the parameters of the DI-Pulse model are fine-tuned to correspond with the first sharp peak of the HRR curve, which is indicative of the combustion of the diesel pilot. This model monitors the complete lifecycle of the diesel fuel, from injection to combustion, by segmenting the fuel into various axial and radial zones. It considers droplet breakup, air entrainment, and evaporation, utilizing calibration factors for ignition delay, premixed combustion, and diffusive combustion. Once the DI-Pulse model is calibrated, the SITurb model is modified to align with the subsequent, broader section of the HRR curve, which is primarily influenced by the turbulent combustion of H_2. This model, grounded in the Blizzard and Keck framework, simulates the transition of the flame from a laminar to a turbulent state.

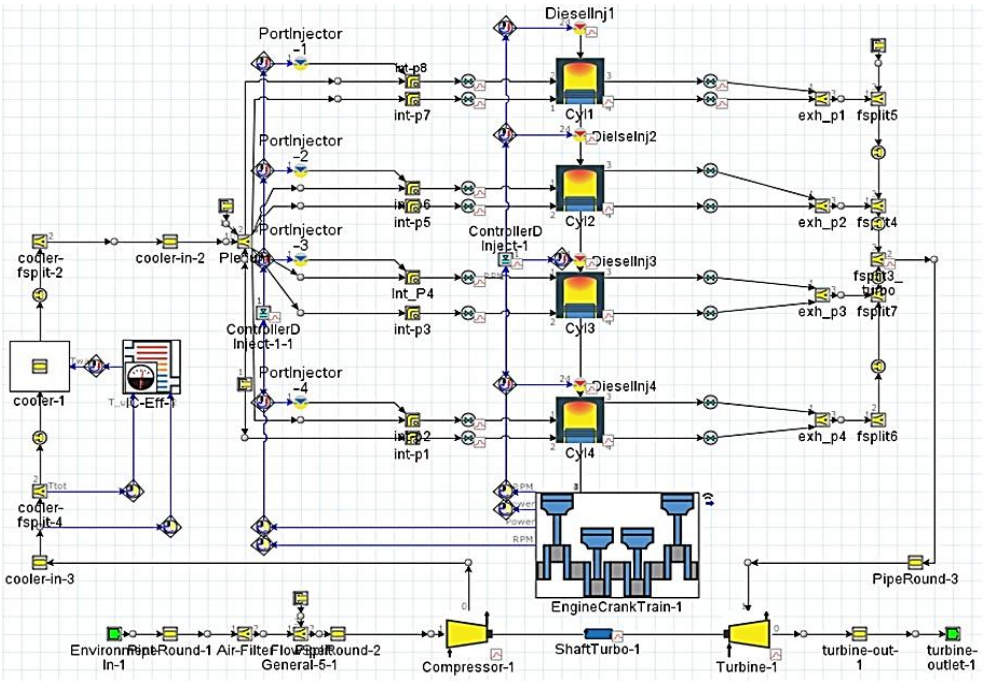

Figure 1. H_2-diesel dual fuel: simulation schematic layout

It computes the rate at which the unburned mixture is drawn into the flame front and the rate at which this mass combusts. The tuning process necessitates an iterative exchange between the two models, as the energy produced from the diesel combustion has a direct impact on the H_2 combustion [20]. This burn rate is computed using the combustion model. Energy equations of unburn and burned zone are mentioned in (1) and (2).

$$\frac{d(m_u e_u)}{dt} = -p\frac{dV_u}{dt} - Q_u - \left(\frac{dm_{f,b}}{dt}h_f + \frac{dm_{a,b}}{dt}h_a\right) + \frac{dm_{f,i}}{dt}h_{f,i} \quad (1)$$

$$\frac{d(m_b e_b)}{dt} = -p\frac{dV_b}{dt} - Q_b - \left(\frac{dm_{f,b}}{dt}h_f + \frac{dm_{a,b}}{dt}h_a\right) \quad (2)$$

Where m_u & m_b represent the masses of the unburned and burned zones, respectively, e_u & e_b denote the energies of the unburned and burned zones, V_u& V_b indicate the volumes of the unburned and burned zones, Q_u & Q_b refer to the heat transfer rates of the unburned and burned zones, p signifies the in-cylinder pressure, t represents time, h_f is the enthalpy of the fuel mass, h_a is the enthalpy of the air mass, $h_{f,i}$ is the enthalpy of the injected fuel mass, $m_{a,b}$ is the mass of air transferred to the burned zone, $m_{f,i}$ is the injected fuel mass, and $m_{f,b}$ is the fuel mass transferred to the burned zone.

2.1.1. "DIPulse" diesel combustion model

The combustion process is governed by key calibration factors such as ignition delay(C_{ign}), premixed combustion and diffusive combustion. The air-entrainment factor (C_{ent}) is calculated according to (3) based on the injector nozzle velocity (u_{inj}) and the subsequent fuel spray breakup time (t_b) to determine the spray tip length (S).

$$\frac{dm}{dt} = -C_{ent}\frac{m_{inj}u_{inj}}{u^2}\frac{du}{dt} \quad (3)$$

$$(S) = \begin{cases} 16\left(\frac{t}{t_b}\right)^{0.5} & \frac{t}{t_b} \le 1 \\ 16 & \left(\frac{t}{t_b}\right) \ge 1 \end{cases} \quad (t_b) = 4.351\sqrt{\frac{2\rho_l}{\rho_g}}\frac{d_n}{C_d u_{inj}} \quad (u_{inj}) = C_d\sqrt{\frac{2\Delta P}{\rho_l}} = \frac{\dot{m}_{inj}}{A_n\rho_l}$$

Where, t is time, S is spray tip length, t_b is breakup time, ρ_g is density of H_2, d_n is diameter of nozzle, C_d is discharge coefficient of nozzle, ρ_l is diesel density, ΔP is nozzle pressure drop, $\dot{m}_{inj}$ is injector out mass flow

rate, A_n is area of nozzle, and u_{inj} is injector nozzle velocity. The ignition delay factor (C_{ign}) is calculated based in (4) based on the ignition delay.

$$(\tau_{ign}) = C_{ign}\rho^{-1.5} exp\left(\frac{3500}{T}\right)(O_2)^{-0.5} \quad (4)$$

$$\int_{t_0}^{t_{ign}} \frac{1}{\tau_{ign}} dt = 1$$

Where, τ_{ign} is ignition delay, (O_2) is concentration of oxygen within the pulse, T is temperature within the pulse, and ρ is gas density within the pulse. Following ignition, the model calculates the rate of premixed charge mass formation ($\frac{dm_{pm}}{dt}$) and the rate of entrained mass formation for diffusive burning ($\frac{dm}{dt}$) the the premixed combustion factor as mentioned in (5) and diffusive combustion factor as mentioned in (6).

$$\left(\frac{dm_{pm}}{dt}\right) = C_{pm} m_{pm} k\left(t - t_{ign}\right)^2 f\left((O_2)\right) \quad (5)$$

$$\left(\frac{dm}{dt}\right) = C_{df} m \frac{\sqrt{k}}{\sqrt[3]{V_{cyl}}} f\left((O_2)\right) \quad (6)$$

Where, t is the current time, t_{ign} is ignition phase duration, m_{pm} is mass of premixed charge, k is premixed stage turbulent flow energy/entrainment stage turbulent kinetic energy, V_{cyl} is entrainment stage cylinder volume, and (O_2) is entrainment stage oxygen concentration. The model accounts for the transition from a spray-dominated combustion to an established flame front. This is achieved by calculating an effective flame area (A_f) as shown in (7).

$$(A_f) = \left(1 - \frac{R_f}{S}\right) A_{spray} + \left(\frac{R_f}{S}\right) A_{flame} \quad (7)$$

Where, A_f is the effective flame area, R_f is the flame front radius or reaction zone thickness, S is the spray tip length, A_{spray} is area of the fuel spray, and A_{flame} is the characteristic area of the flame.

2.1.2. "SITurb" - H_2 combustion model

The characteristic burning time (τ_b) is determined by the laminar flame speed (u_L) as per in (8) and the turbulent burning velocity (u_T) is calculated to describe the flame propagation as per (9). The model calculates the rate at which the unburned mixture is entrained into the flame front and the rate at which this mass burns. Rate of mass entrainment calculated as per in (10) into the flame front ($\frac{dM_e}{dt}$) and then determines the final rate of burned mass formation ($\frac{dM_b}{dt}$) as per in (11) based on the entrained mass (M_e) and the burning time (τ_b).

$$(\tau_b) = \frac{\lambda}{u_L} \quad (8)$$

$$(u_T) = C_{TFS} u' \left(1 - \frac{1}{1 + C_{FKG}\left(\frac{R_f}{L}\right)^2}\right) \quad (9)$$

$$\left(\frac{dM_e}{dt}\right) = \rho_u A_{FF} u_{te} \quad (10)$$

$$\left(\frac{dM_b}{dt}\right) = \frac{M_e - M_b}{\tau_b} \quad (11)$$

Where, τ_b is the burning time, λ is characteristic length scale, u_L is laminar flame speed, u' is turbulent fluctuating velocity, C_{TFS} is turbulent flame speed multiplier, C_{FKG} is flame kernel growth multiplier, R_f is flame radius, L is integral length scale of turbulence, M_e is entrained mass, ρ_u is entrainment stage unburned mixture density, A_{FF} is area of flame front at entrainment stage, u_{te} is entrainment stage turbulent velocity, M_e is entrained mass, $M_b$is burned mass, and τ_b is burning time.

2.1.3. Apparent heat release rate (AHRR)

Net HRR calculated as per (12) as a function of crank angle [21]. This curve represents the combined energy release from both the diesel and H_2 combustion phases.

$$AHRR = \left(-p\frac{dV}{dt} - \frac{dQ}{dt} - \frac{d(me_s)}{dt} + \Sigma_i \dot{m}_i h_{i,s}\right) \quad (12)$$

Where $p\frac{dV}{dt}$ is the rate of work done by the system, $-\frac{dQ}{dt}$ is the rate of heat transfer out of the system, $-\frac{d(me_s)}{dt}$ is the rate of change of sensible energy of the mass within the system, $-\Sigma_i \dot{m}_i h_{i,s}$ is the sum of the enthalpy flows associated with the sensible energy of mass crossing the system boundary, $\dot{m}_i$ is the mass flow rate of species 'i', and $h_{i,s}$ is the specific sensible enthalpy of species 'i'.

2.2. Experimental setup for validating combustion model

For the experimental study, a four-cylinder diesel engine was modified to operate on a dual-fuel mixture of H_2-diesel. Table 1 and Figure 2 depict the engine specifications and the schematic layout of the experimental setup. H_2 was introduced into the intake port through injectors after its pressure was reduced from 250 bar to a level of 2 bar. Diesel acted as the pilot fuel, igniting under compression to initiate the combustion of the H_2-air mixture. Experiments were carried out at four distinct engine loads (4, 8, 12, and 16 bar BMEP), with measurements taken for pure diesel operation as a baseline, followed by tests with H_2 contributing 25% of the total energy input. The H_2 injection was optimized to occur during the intake stroke to ensure a homogeneous mixture and to prevent gas from escaping.

Table 1. Engine specification

Parameter	Unit	Value
Engine make	---	KOEL – 4 cylinders
Bore x stroke	mm	105 x 125
Displacement	Ltr	4.32
Rating	kW	86 kW @ 1500 rpm
Firing order	---	1-3-4-2
Compression ratio	---	15.5 :1
Pilot fuel	---	Diesel
Pilot fuel timing	° BTDC	15° ± 1

The duration of H_2 injection varied from 15.0 °CA to 74.9 °CA for flow rates ranging from 0.5 kg/hr to 2.5 kg/hr. The optimal injection timing was determined to be 45° after gas exchange TDC, which aligns with previous research [22], [23]. Detailed instrumentation list presented in Table 2. Each experiment was repeated three times to ensure reliability, and an uncertainty analysis was conducted to evaluate the overall accuracy, similar to a previous study [24]. The results of the experimental uncertainty are presented in Table 3, while the equipment uncertainty is shown in Table 4. Essential instrumentation, such as pressure and temperature, along with safety measures, such as non-return valves, flame traps, and flame arrestors, have been integrated into the H_2 supply line as shown in Table 2.

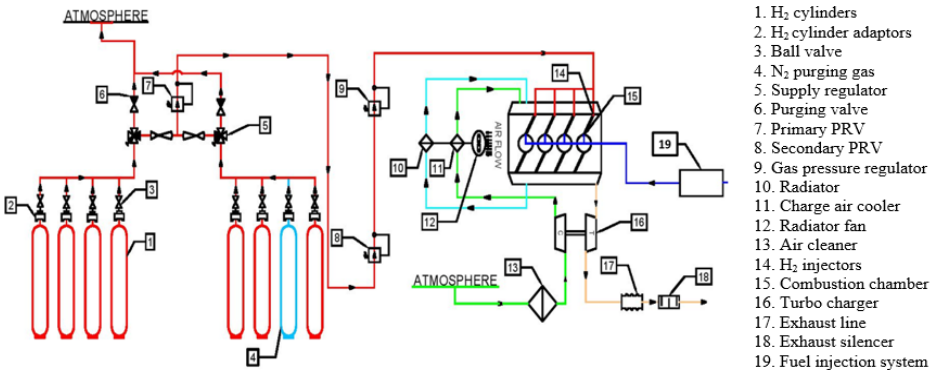

Figure 2. H_2-diesel dual fuel: experimental schematic layout

Table 2. Instrumentation

System	Description	Make	Range	Accuracy
H_2 Gas flow	First stage pressure regulator	GCE	10-250 bar	±1.0% of FS
	2nd stage pressure regulator	VANAZ	10-250 bar	±1.0% of FS
	H_2 line Pressure gauge	GCE	0-3 bar, 0-15 bar	±1.0% of FS
	H_2 Leak detecting sensors	AMBETRONIC	0-100% H_2	±1.0% of FS
	H_2 - Flow meter	Aalborg	0-10 kg /hr.	±1.0% of FS
	Gas flash back arrestor	DEMAX	0-5.0 bar, 0-15 bar,	±1.0% of FS
Diesel flow	Diesel flow meter	AVL 735	0-100 cc	±1.0% of FS
Air flow	Venturi flow meter	Eureka	0-800 m3/hr.	±1.0% of FS
Pressure	Pressure sensors	DRUCK	0-5 bar	±1.0% of FS
Temperature	Temperature sensors	Hi-Tech	RTD and Thermocouple	± 0.8 °C up to 200 °C
Emission	Emission analyser	HORIBA MEXA 584L	NO: 0-5000 ppm	1 ppm
			HC: 0-10000 ppm	>2000 ppm, 1 ppm
			CO_2: 0-20%	0.1% vol
In-cylinder pressure	Combustion system	AVL INDICOM	720 °CA	±0.5 °CA
	6045 A piezoelectric sensor	Kistler	0 ... 250 bar	20 pC/bar

Table 3. Emission parameters uncertainty analysis

Pollutant	Average reading	% Random uncertainty	% Instrument uncertainty	Total measurement uncertainty (%)
HC (PPM)	85	4.71%	1.70%	2.17%
NOx (PPM)	634	4.25%	1.70%	1.99%
CO (PPM)	99.3	0%	1.70%	1.70%
CO_2 (%)	8.1	3.02%	1.70%	1.88%

Table 4. Performance parameters uncertainty analysis

Parameter	Unit	Uncertainty
Voltage	V	±2
Current	A	±1
Diesel mass flow	kg/s	$\pm 5.4 \times 10^{-5}$
H_2 mass flow	kg/s	$\pm 3.3 \times 10^{-6}$
Total fuel consumption	kg/s	$\pm 5.4 \times 10^{-5}$

2.3. Model validation

A detailed validation of computational models for both diesel and dual-fuel engines was performed by comparing simulation results with experimental data for 4, 8, 12, and 16 bar BMEP with 25% H_2 energy substitution. The graphical depiction of in-cylinder pressure, heat release rate (HRR), and combustion phases at 12 bar BMEP for both diesel and dual fuel modes is illustrated in Figures 3(a) and 3(b), Figures 4(a) and 4(b) for enhanced comprehension. The result shows a strong correlation between simulated and experimental in-cylinder pressure, HRR and combustion phases for both “DI pulse” and combine "DIPluse + SITurb" dual fuel model. The validation confirmed that both models are highly accurate, with an absolute error for in-cylinder pressure within ±5% and a combustion phase prediction error within ±2 °CA. This robustly validated dual-fuel model was then used to simulate a wider range of operating conditions. The consistency in matching curve shapes and peak values across all tested BMEP levels confirms the models' reliability.

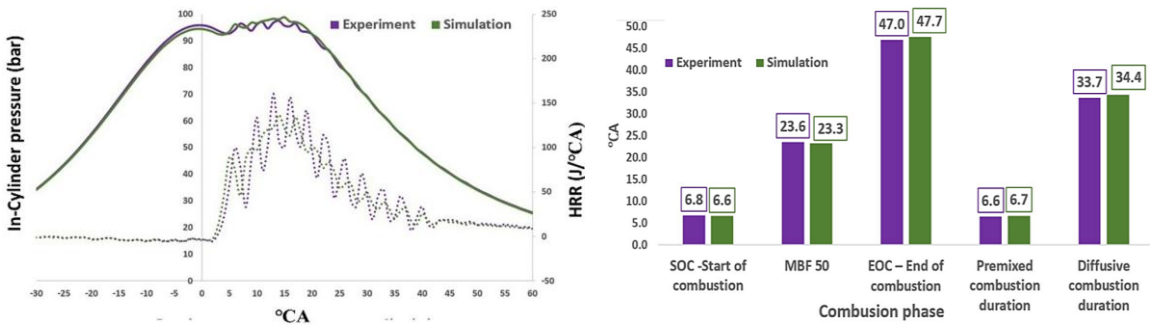

Figure 3. Model validation comparing simulation and experimental results for diesel mode at 12 bar BMEP, showing (a) in-cylinder data and (b) combustion phase details

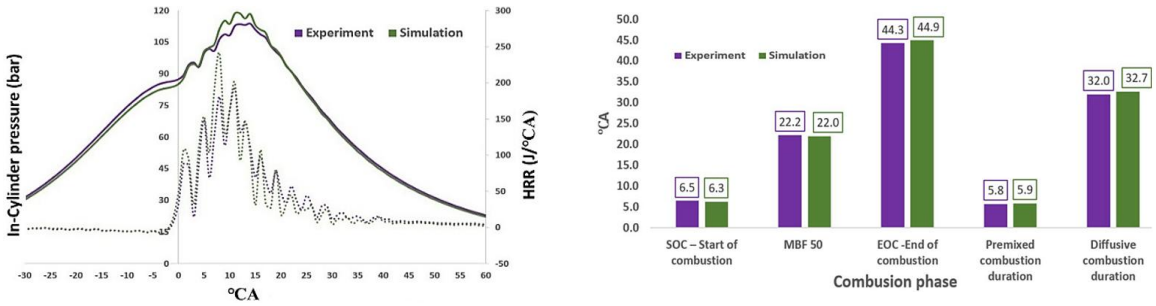

Figure 4. Model validation comparing simulation and experimental results for dual fuel mode at 12 bar BMEP, showing (a) in-cylinder data and (b) combustion phase details

2.4. Response surface methodology (RSM) statistical analysis

To optimize engine performance and emissions, a response surface methodology (RSM) was utilized with a Box-Behnken experimental design [9], [13], [14] as per DoE mentioned in Table 5. The study analyzed influence of three independent factor such as engine load (BMEP), lower calorific value of fuel (LCV) and H_2. energy substitution on response factors like BTE and BSFC, as well as on the emissions including NO_x, HC, CO, and CO_2. Using ANOVA, a quadratic polynomial equation was developed and validated with statistical metrics like R^2, Adj-R^2, and Pred-R^2. The model's strong fit, with an R^2 value over 80%, confirmed its accuracy for predicting engine behavior and identifying optimal operating conditions.

2.5. Random forest machine learning

This research utilized RF algorithm to predict the performance of a dual-fuel engine [16], [25]. Figure 5 shows the model was built using orange data mining (v3.3) and trained on a normalized dataset of 90 unique data points, which were split into a 70% training set (60 points) and a 30% testing set (30 points). The RF model was designed to predict seven key outputs which are BTE, BSFC, NO_x, HC, CO, and CO_2. The inputs used to make these predictions BMEP, LCV, and H_2 substitution. The core of the model is ensemble learning and bagging, which involves building a "forest" of multiple decision trees.

Each tree was trained on a different random subset of the training data created through bootstrap sampling. To further enhance diversity and prevent overfitting, the current model used the random subspace method, which considers only a random subset of 2 features at each split within a tree. Table 6 shows the hyperparameters for the model were set as follows: 70 trees (n_estimators), maximum tree depth of 7 (max_depth), and a minimum of 3 samples per split (min_samples_split). The model's performance was evaluated using 10-fold cross-validation and a variety of metrics. Key metrics included mean squared error (MSE), root mean squared error (RMSE), and the coefficient of determination (R^2) [26], [27]. A successful model was defined as having an R^2 value of 0.9 or greater, indicating a strong fit with minimal difference between the training and testing results. To combat overfitting, the study leveraged the RF model's inherent randomness in both data sampling and feature selection. Additionally, hyperparameter tuning was performed by adjusting the max_depth, min_samples_leaf, and n_estimators to ensure the model wasn't overly complex and could generalize well to new data.

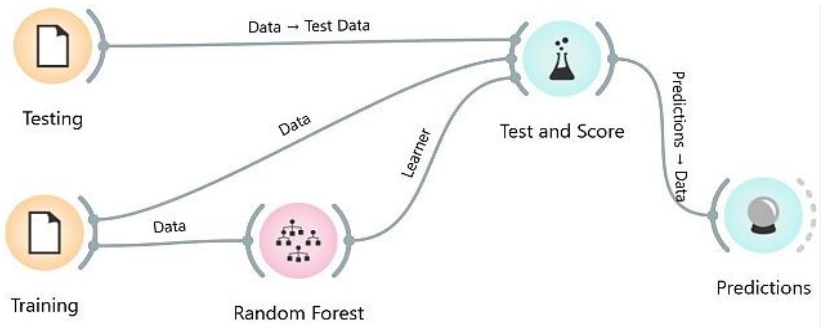

Figure 5. Orange data mining layout: random forest

Table 5. RSM model - DOE

	BMEP (bar)	LCV (kJ/kg)	H_2 %	Response
Level 01	2	43500	0	BTE (%)
Level 02	4	46462	10	BSFC
Level 03	6	49857	20	(g/kw.hr)
Level 04	8	53787	30	NO_x (ppm)
Level 05	10	58389	40	CO (ppm)
Level 06	12	63853	50	HC (ppm)
Level 07	14	70445	60	CO_2 (ppm)
Level 08	16	78555	70	

Table 6. Hyper parameters

Parameters	Selected
Criterion	gini
n_estimators	70
max_depth	7
min_samples_split	3
min_sample_leaf	1
max_features	sqrt

3. RESULTS AND DISCUSSION

3.1. Brake thermal efficiency (BTE, %)

The contour plot in Figure 6 demonstrates the connection between BTE (%), the percentage of H_2 (H_2-%), used as substitution fuel and BMEP (bar). Increasing H_2 substitution up to 40% boosts BTE by about 1% for every 10% of H_2 added. The highest BTE is achieved when both engine load (BMEP) and H_2 substitution are high. A peak efficiency of 41% was recorded at 40% H_2 and 14 bar BMEP, a 3% improvement over pure diesel. Furthermore, a 2.5% BTE increase is possible without raising NO_x emissions. The observed results are similar to the previous research [28], [29]. Beyond 40% H_2 substitution BTE starts declines from 41% to 38% similar to preivous published results [30]. The anticipated reasons for decrease in BTE is mainly due to combination of factors, including combustion phasing, reduced volumetric efficiency, and increased heat loss. H_2 displaces a portion of the incoming air for the same volume and decreases the total mass of the charge [31]. This reduction in the mass of the charge also further support along to a lower BTE [32].

Regression in (13) is a quadratic model of RSM that predicts BTE (%) based on three independent variables: BMEP (bar), the percentage of H_2 substitution (H_2-%), LCV (kJ/Kg). Table 7 provides the model's performance of both RSM and RF. Figure 7 depicts the cross-validation process used to evaluate the model by training and testing it on various subsets of the data multiple times. RF model provides highly accurate and consistent predictions, making it a much more suitable and trustworthy model than RSM model.

$$BTE\ (\%) = 24.7 + 1.36\,BMEP + 0.112\,H_2 - \% + 0.00004\,CV - 0.0078\,BMEP * BMEP - 0.00037\,H_2 - \% * H_2 - \% + 0.000000\,CV * CV + 0.0129\,BMEP * H_2 - \% - 0.000019\,BMEP * CV - 0.000004\,H_2 - \% * CV \quad (13)$$

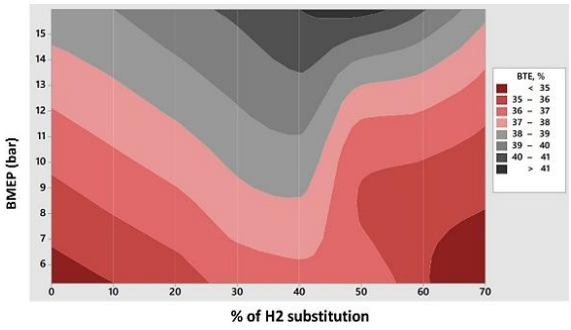

Figure 6. Change in BTE (%) with respect to H_2 subtitution (%) and BMEP (bar)

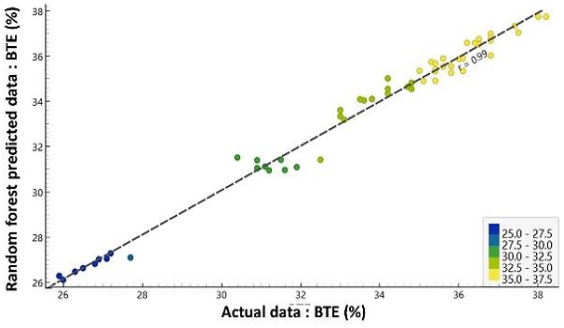

Figure 7. Cross-validation: random forest-BTE (%)

Table 7. Model accuracy -BTE, %

Metric	RSM model	RF model
R^2 (train)	0.9391	0.998
R^2 (test/predicted)	0.7703	0.979
Cross-validation R^2	-	0.984

3.2. Brake specific fuel consumption (BSFC, g/kW.hr)

Figure 8 shows the contour plot on the relationship between BSFC, BMEP, and the percentage of H_2 (H_2-%). An increase in H_2 substitution reduces BSFC of approximately 10 g/kW.hr for every 10% of H_2 energy substitution. Specifically, a substitution rate of 40% H_2 results in a decrease in BSFC by 80 g/kW when compared to pure diesel. However, in order to maintain the same NO_x emissions as pure diesel, the improvement in BSFC is limited to 40 g/kW.hr, which represents an 18% reduction relative to pure diesel for a 25% H_2 substitution. The noted reduction in BSFC with H_2 substitution directly reflects the enhanced thermal efficiency of the engine. The improved combustion characteristics facilitate a more efficient conversion of fuel energy into power, thereby requiring less fuel for each kilowatt-hour of energy produced. The results obtained are consistent with findings from previous studies [10], [33].

Regression (14) is a quadratic model of RSM that predicts BSFC (g/kW.hr) based on three independent variables: BMEP (bar), the percentage of H_2 substitution (H_2-%), and LCV (kJ/Kg). Table 8 provides the model's performance of both RSM and RF. Figure 9 depicts the cross-validation process used to evaluate the model by training and testing it on various subsets of the data multiple times. Both RSM and RF model provides highly accurate and consistent predictions, making it a much more suitable with exceptional predictive capability on unseen test data.

$$BSFC(g/kWhr) = 286 - 4.06\,BMEP - 1.52\,H_2 - \% - 0.00086\,CV + 0.0380\,BMEP * BMEP + 0.0115\,H_2\% * H_2\% + 0.000000\,CV * CV - 0.0096\,BMEP * H_2 - \% + 0.000022\,BMEP * CV - 0.000007\,H_2\% * CV \quad (14)$$

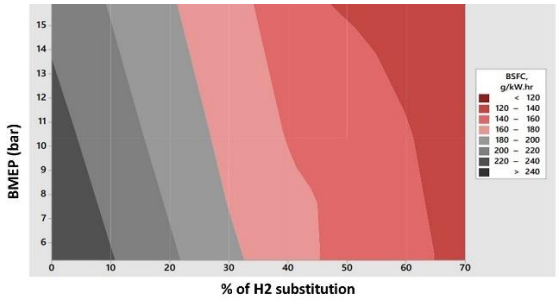

Figure 8. Change in BSFC (g/kW.hr) with respect to H_2 subtitution (%) and BMEP (bar)

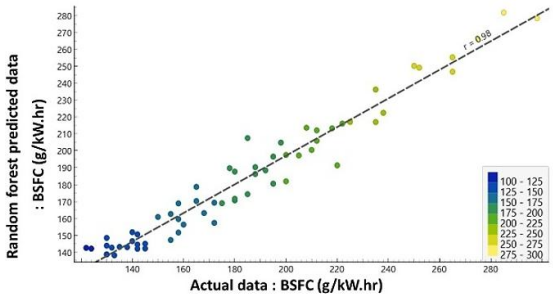

Figure 9. Cross-validation: random forest – BSFC (g/kW.hr)

Table 8. Model accuracy-BSFC, g/kW.hr

Metric	RSM model	RF model
R^2 (train)	0.99	0.99
R^2 (test/predicted)	0.98	0.99
Cross-validation R^2	-	0.94

3.3. Nitrogen oxide (NO_x, PPM)

The contour plot illustrated in Figure 10 depicts the correlation between NO_x (PPM), the percentage of H_2 substitution (H_2-%) and BMEP (bar). This research utilized a compression ratio of 15:1, and it was found that with a combination of low CR and H_2 substitution at or below 25%, NO_x emissions remain relatively stable, irrespective of the BMEP. A similar finding was reported in a prior study, which indicated that the addition of H_2 had a negligible impact on NO_x emissions at 20% and 40% [34]. Another investigation also noted a minor reduction in NO_x emissions with small quantities of H_2 addition [35]. However, when H_2 substitution exceeds the 25% threshold, there is a significant increase in NO_x emissions. This rise is particularly notable for all the BMEP levels, where NO_x emissions surge by approximately 200 ppm. This incremental rise in NO_x is attributed to the fact that the combustion of H_2 can occur across a broad spectrum of air-fuel ratios,

and the combustion of a rich air-H_2 mixture at elevated temperatures fosters an optimal environment for the formation of NO_x emissions [36]. Although a 30-40% H_2 substitution was found to be optimal for other performance and emission factors, it led to higher NO_x emissions. Therefore, a 25% H_2 substitution is recommended as a practical compromise. This level provides most of the benefits of higher substitution rates while keeping NO_x emissions low, aligning with the goal of maintaining NO_x levels similar to conventional diesel engines. NO_x emission primarily driven by combustion phasing and oxygen availability. By controlling these parameters, NO_x levels can be kept comparable to conventional diesel engines [37].

Regression (15) is a quadratic model of RSM that predicts NO_x (PPM) based on three independent variables: BMEP (bar), the percentage of H_2 substitution (H_2-%), and LCV (kJ/Kg). Table 9 provides the model's performance of both RSM and RF. Figure 11 depicts the cross-validation process used to evaluate the model by training and testing it on various subsets of the data multiple times. Both RSM and RF model provides highly accurate and consistent predictions, making it a much more suitable with exceptional predictive capability on unseen test data.

$$NOx\ (ppm) = 2704 - 180.0\ BMEP + 34.9\ \% - 0.0278\ CV + 9.81\ BMEP * BMEP + 0.697\ H_2\% * H_2\% + 0.000000\ CV * CV - 0.938\ BMEP * H_2\% - 0.00096 BMEP * CV - 0.000521\ H_2\% * CV \quad (15)$$

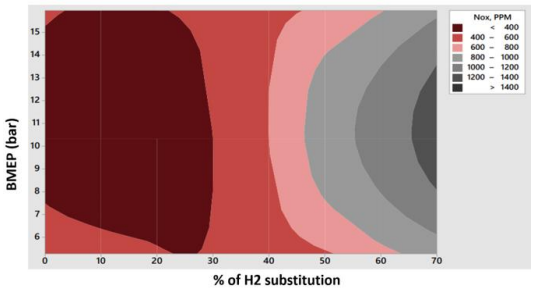

Figure 10. Change in NOx (PPM) with respect to H_2 subtitution (%) and BMEP (bar)

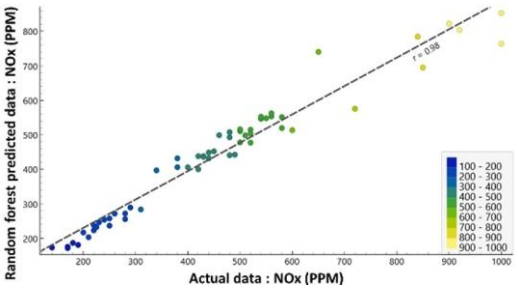

Figure 11. Cross validation: random forest – Nox (PPM)

Table 9. Model accuracy - NO_x, PPM

Metric	RSM model	RF model
R^2 (train)	0.98	0.98
R^2 (test/predicted)	0.94	0.98
Cross-validation R^2	-	0.92

3.4. Hydrocarbon (HC, PPM)

The contour plot presented Figure 12 shows the relationship between HC (PPM), the percentage of H_2 substitution (H_2-%) and BMEP (bar). HC emissions remain unchanged when H_2 substitution is at or below 10%, irrespective of the brake mean effective pressure (BMEP). Once the H_2 substitution surpasses the 10% threshold, a gradual reduction in HC emissions commences. For each 1% rise in H_2 substitution beyond 10%, HC emissions diminish by 10 ppm. This decrease becomes even more significant when H_2 substitution goes beyond 20%. To achieve NO_x-neutral operation, a 20% reduction in HC emissions is the maximum benefit observed, which occurs at a 25% H_2 substitution rate. Adding H_2 to fuel reduces unburnt HC emissions by making combustion complete and more efficient. This happened because of higher combustion temperatures helped to burn up residual hydrocarbon fuel left over from the initial combustion phase. Faster flame speed ensured the fuel-air mixture is consumed rapidly and thoroughly, leaving less unburnt fuel to escape into the exhaust. Enhanced oxidation hydroxyl radicals (OH) molecules actively break down and oxidize stubborn hydrocarbon molecules, ensuring they are fully burned. Wider Flammability Range of H_2 burn in a wider range of air-to-fuel ratios than diesel. This allows it to burn in pockets of the cylinder where the mixture might be too lean or too rich for diesel to combust on its own, thereby reducing pockets of unburnt fuel. A similar observation was made by a researcher who found that with an 18% H_2 mass share in a compression-ignition (CI) engine running in dual-fuel mode, HC emissions were considerably lower compared to a pure diesel mass share. Specifically, at full load, HC emissions dropped from 130 ppm to 70 ppm, and at 20% load, they

decreased from 40 ppm to 20 ppm [34]. Another study also reported comparable results, indicating a substantial reduction in HC emissions to approximately 1 g/kWh [36].

Regression (16) is a quadratic model of RSM that predicts HC (PPM) based on three independent variables: BMEP (bar), the percentage of H2 substitution (H_2-%), LCV (kJ/Kg). Table 10 provides the model's performance of both RSM and RF. Figure 13 depicts the cross-validation process used to evaluate the model by training and testing it on various subsets of the data multiple times. Both RSM and RF model provides highly accurate and consistent predictions, making it a much more suitable with exceptional predictive capability on unseen test data.

$$HC\ (ppm) = 112 - 1.81\ BMEP + 2.19\ H_2\% - 0.00403\ CV - 0.416\ BMEP * BMEP + 0.0192\ H_2\% * H_2\% + 0.000000\ CV * CV + 0.0217\ BMEP * H_2\% + 0.000121\ BMEP * CV - 0.000088\ H_2\% * CV \quad (16)$$

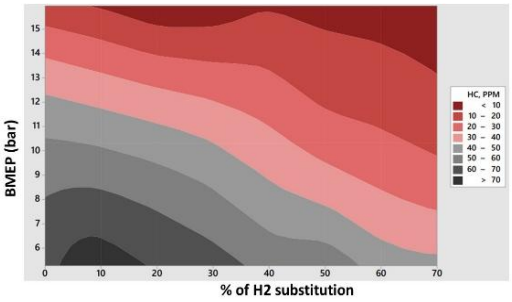

Figure 12. Change in HC (PPM) with respect to H_2 substitution (%) and BMEP (bar)

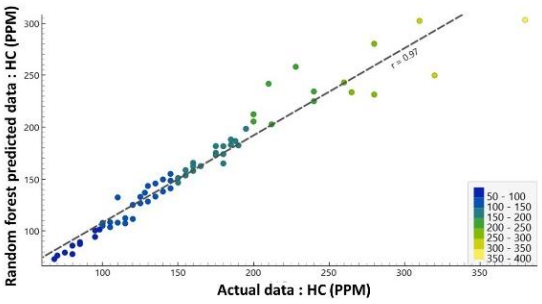

Figure 13. Cross-validation: random forest HC (PPM)

Table 10. Model accuracy -HC, PPM

Metric	RSM model	RF model
R^2 (train)	0.98	0.99
R^2 (test/predicted)	0.95	0.98
Cross-validation R^2	-	0.93

3.5. Carbon di-oxide (CO_2, %)

The contour plot presented in Figure 14 shows the relationship between CO_2 (%), the percentage of H_2 substitution (H_2-%) and BMEP (bar). In this research, carbon dioxide (CO_2, %) emissions progressively decline as the percentage of H_2 substitution rises. This pattern initiates at 5% H_2 substitution, with CO_2 decreasing by 1% for every 10% increase in H_2 up to 30%. After this threshold, additional H_2 substitution does not influence CO_2 levels.

The optimal range for H_2 substitution is identified as being between 25% and 35%, resulting in an average CO_2 reduction of 3%. These results are consistent with earlier studies, which indicated a significant decrease in CO_2 emissions—from 920 g/kWh to approximately 240 g/kWh—when a 7.5% H_2 volume share was utilized in comparison to pure diesel [38]. The CO_2 emission trends observed in this research also reflect the trends in CO emissions, where reductions in both gases are associated with a decrease in the consumption of carbon-based fuels [39]. A linear correlation was noted between the increase in H_2 energy share and the reduction in CO_2 emissions. The current research findings are comparable to previous studies where a 40% H_2 energy substitution led to a 40% decrease in CO_2 [37].

$$CO2\ (\%) = 23.5 - 0.161\ BMEP + 0.301\ H2\% - 0.000726\ CV + 0.00509\ BMEP * BMEP + 0.00373\ H2\% * H2\% + 0.000000\ CV * CV - 0.00182\ BMEP * H2\% + 0.000004\ BMEP * CV - 0.000009\ H2\% * CV \quad (17)$$

Regression (17) is a quadratic model of RSM that predicts CO_2 (%) based on three independent variables: BMEP (bar), the percentage of H_2 substitution (H_2-%), LCV (kJ/Kg). Table 11 provides the model's performance of both RSM and RF. Figure 15 depicts the cross-validation process used to evaluate the model by training and testing it on various subsets of the data multiple times. Both RSM and RF model provides highly accurate and consistent predictions, making it a much more suitable with exceptional predictive capability on unseen test data.

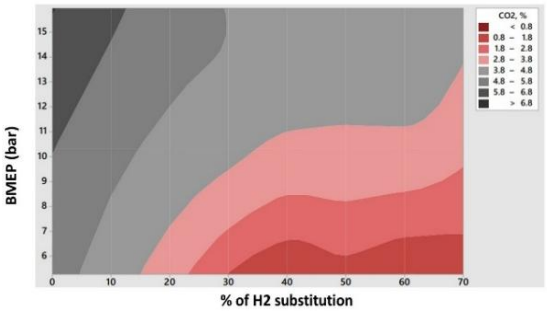

Figure 14. Change in CO_2 (%) with respect to H_2 subtitution (%) and BMEP (bar)

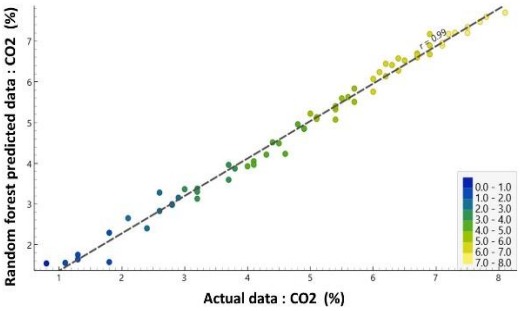

Figure 15. Cross-validation: random forest CO_2 (%)

Table 11. Model accuracy - CO_2 (%)

Metric	RSM model	RF model
R^2 (train)	0.99	0.99
R^2 (test/predicted)	0.95	0.99
Cross-validation R^2	-	0.98

3.6. Carbon monoxide (CO, PPM)

The contour plot presented in Figure 16 shows the relationship between CO (PPM), the percentage of H_2 substitution (H_2-%) and BMEP (bar). Increasing the H_2 substitution rate in a dual-fuel diesel engine can significantly reduce CO emissions. Up to a 20% H_2 substitution rate, CO emissions remain unchanged. However, once the substitution exceeds this threshold, emissions begin to drop sharply. For every 10% increase in H_2 substitution, CO emissions decrease by about 50 ppm across all engine loads. The most effective range for reducing CO is between 40% and 50% H_2 substitution, which can lead to a total reduction of 200–250 ppm. To achieve NO_x-neutral operation, a 50-60 ppm reduction in CO emissions is the maximum benefit observed, which occurs at a 25% H_2 substitution rate. This is because H_2 promotes more complete combustion by increasing temperatures and producing hydroxyl (OH) radicals that convert CO to CO_2. Additionally, hydrogen's faster flame speed and ability to burn in leaner mixtures prevent the initial formation of CO. These results are consistent with earlier studies. For example, at 100% load, CO emissions decreased from 3.14 g/kWh in standard diesel mode to 2.31 g/kWh with a 10.1% H_2 energy share in dual-fuel mode [39]. Another study reported nearly zero CO emissions with approximately 28% H_2 mass share in a CI engine at 20%, 40%, and 60% loads [34].

Regression (18) is a quadratic model of RSM that predicts CO (PPM) based on three independent variables: BMEP (bar), the percentage of H2 substitution (H_2-%), LCV (kJ/Kg). Table 12 provides the model's performance of both RSM and RF. Figure 17 depicts the cross-validation process used to evaluate the model by training and testing it on various subsets of the data multiple times. Both RSM and RF model provides highly accurate and consistent predictions, making it a much more suitable with exceptional predictive capability on unseen test data.

$$CO\ (ppm) = 419 - 12.5\ BMEP - 6.84\ H2\% - 0.0017\ CV + 0.335\ BMEP * BMEP + 0.0436\ H2\% * H2\% + 0.000000\ CV * CV + 0.221\ BMEP * H2\% - 0.000151\ BMEP * CV - 0.000008\ H2\% * CV \quad (18)$$

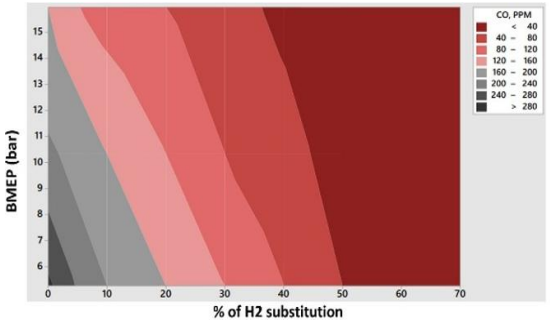

Figure 16. Change in CO (PPM)with respect to H_2 substitution (%) and BMEP (bar)

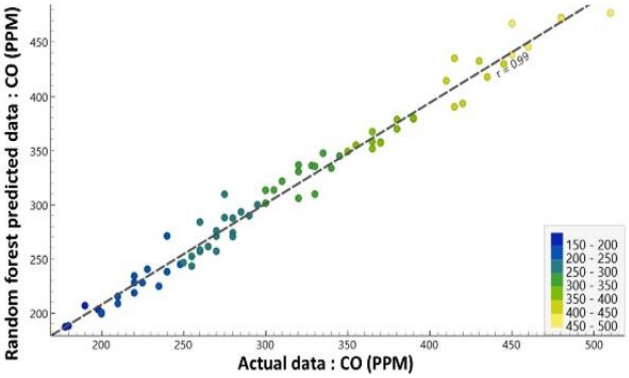

Figure 17. Cross-validation: random forest CO (PPM)

Table 12. Model accuracy-CO (PPM)

Metric	RSM model	RF model
R^2 (train)	0.99	0.99
R^2 (test/predicted)	0.97	0.99
Cross-validation R^2	-	0.98

3.7. Result comparison

Tables 13 and 14 present a comprehensive overview of the consolidated results. Table 13 compares the current findings with those of previous studies. While Table 14 specifically focuses on comparing the machine learning predictions with earlier research.

Table 13. Comparison of current research result with previous researches

Author	Engine configuration			Optimal H_2	% of change						
	No cylinder	Speed rpm	BMEP bar	substitution %	BTE %	BSFC g/kW.hr	NO_X PPM	HC PPM	CO PPM	CO_2 %	Soot g/kW.hr
[40]	4	2250	8	7.5%	5.0%	1.2%	17.0%	28.0%	20.0%	8.2%	X
		1750	9	7.5%	2.0%	5.5%	22.0%	22.0%	16.0%	9.3%	X
		1250	10	7.5%	2.5%	9.5%	26.0%	31.0%	20.0%	9.3%	X
[41]	4	1500	11	20.0%	4.5%	25.0%	7.5%	11.0%	5.0%	15.0%	2.5%
[11]	4	2200	5	17.5%	7.0%	24.0%	47.0%	X	X	X	X
		2000	8	17.5%	6.0%	18.0%	50.0%	X	X	X	X
		1500	12	17.5%	10.0%	16.0%	28.0%	X	X	X	X
		1000	14	17.5%	15.0%	1.0%	61.0%	X	X	X	X
[42]	4	1500	6	80.0%	3.0%	22.0%	90.0%	20.0%	80.0%	60.0%	95.0%
[43]		1500	13	40.0%	3.0%	X	24.0%	2.0%	4.0%	X	X
Current	4	1500	16	25.0%	2.0%	18.0%	Neutral	20.0%	40.0%	25.0%	4.0%

Table 14. Machine learning model prediction results of previous literature vs current research comparison

Reference	Model inputs (features)	Model outputs (targets)	Model prediction
[44]	% of H_2, load, speed	CO_2, CO, NO_x	Overall R^2= 0.89-0.98
[45]	Fuel injection angles, air-fuel ratio, diesel-to-gas exchange rates, fuel rail pressure	NO_x, CO_2, THC, BTE, smoke	Overall R^2=0.965
[27]	Biogas flow rate, methane fraction (MF), torque, intake temperature	BTE, HC, CO, NO_x, smoke, Secondary fuel energy ratio	Overall model R^2=0.997
[46]	Load, brake power (BP), NO_x, CO_2, exhaust gas temperature (EGT)	BTE	Overall R^2=0.99
[47]	NO_x, RPM, HC, fuel composition	CO	Overall R^2=0.89
[48]	Spark advance, fuel-air ratio, engine speed	IMEP	Overall R^2=0.90
[18]	Spark timing, equivalence ratio, engine speed	BTE, combustion phasings	Not specified
Current research	BMEP, H_2 substitution %, and CV	BTE, BSFC, HC, CO, CO_2, NO_X	Overall R2=0.95-0.99

4. CONCLUSION

Hydrogen as a dual fuel in diesel engines offers a promising approach to improve performance and reduce emissions, though it comes with a trade-off: NO_x emissions. This study used a four-cylinder, 86 kW engine found that increasing H_2 substitution leads to notable gains in engine efficiency and a reduction in most

harmful emissions. The research showed that for every 10% of H_2 added, the BTE increased by about 1%, peaking at 41% with a 40% substitution rate. Beyond this, efficiency declined due to incomplete combustion. Similarly, BSFC decreased by approximately 10 g/kW for every 10% of H_2 added. CO_2, CO, and HC were significantly reduced. CO_2 emissions decreased by 1% for every 10% of H_2 up to a 30% substitution. CO and HC emissions saw sharp reductions once H_2 substitution exceeded 20% and 10%, respectively. However, a critical trade-off was observed with NOx. Emissions remained stable up to a 25% H_2 substitution rate but increased sharply by about 200 ppm beyond this point. For this reason, the study recommends a 25% substitution as a practical compromise, as it increases BTE by 2.5% while maintaining NO_x levels comparable to a conventional diesel engine.

The study used a validated GT-Power simulation model combined with RSM and a RF machine learning algorithm to efficiently analyse engine performance. The RF model provided the prediction accurate with R^2 value of 0.98, 0.99, 0.98, 0.98, 0.99 and 0.99 for BTE, BSFC, NO_x, HC, CO_2, and CO respectively, which significantly reduced the need for extensive physical testing. The proposed solution involves a straightforward retrofitting process using a PFI technique for H_2 and a single-pulse, fixed-timing diesel pilot fuel injection system. This allows the existing engine architecture to be retained without complex modifications. This approach enables increased H_2 substitution (up to 25% at 16 bar) while maintaining NO_x levels around 450 ppm, similar to pure diesel. The results meet several regulatory standards, including India's CPCB-II and internation IMO Tier II and III.

Future research could explore flexible diesel injection strategies to better control NO_x emissions at higher H_2 substitution rates. It would also be beneficial to investigate the combined use of H_2 enrichment with exhaust gas treatment (EGT) systems to further reduce pollutants. Expanding the engine speed range and developing a multi-objective optimization model could provide a more comprehensive understanding and help find the best balance of performance and emissions.

FUNDING INFORMATION

No funding is available to carry out this research work.

AUTHOR CONTRIBUTIONS STATEMENT

This journal uses the Contributor Roles Taxonomy (CRediT) to recognize individual author contributions, reduce authorship disputes, and facilitate collaboration.

Name of Author	C	M	So	Va	Fo	I	R	D	O	E	Vi	Su	P	Fu
Jayagopal Narayanan	✓	✓	✓	✓		✓			✓					
Y. V. V. Satyanarayana Murthy		✓				✓		✓	✓	✓	✓	✓		
Sandeep Kumar						✓				✓				
Talari Surendra					✓				✓					
Ram Mohan Rao Madaka				✓	✓					✓				

C : **C**onceptualization
M : **M**ethodology
So : **So**ftware
Va : **Va**lidation
Fo : **Fo**rmal analysis
I : **I**nvestigation
R : **R**esources
D : **D**ata Curation
O : Writing - **O**riginal Draft
E : Writing - Review & **E**diting
Vi : **Vi**sualization
Su : **Su**pervision
P : **P**roject administration
Fu : **Fu**nding acquisition

CONFLICT OF INTEREST STATEMENT

All the authors reports there is no potential conflict of interest.

DATA AVAILABILITY

Data can be provided on request.

REFERENCES

[1] K. R. Bukkarapu and A. Krishnasamy, "Evaluating the feasibility of machine learning algorithms for combustion regime classification in biodiesel-fueled homogeneous charge compression ignition engines," *Fuel*, vol. 374, p. 132406, Oct. 2024, doi: 10.1016/j.fuel.2024.132406.

[2] V. Beschkov and E. Ganev, "Perspectives on the development of technologies for hydrogen as a carrier of sustainable energy," *Energies*, vol. 16, no. 17, p. 6108, Aug. 2023, doi: 10.3390/en16176108.

[3] S. O. Akpasi, I. M. Smarte Anekwe, E. K. Tetteh, U. O. Amune, S. I. Mustapha, and S. L. Kiambi, "Hydrogen as a clean energy carrier: advancements, challenges, and its role in a sustainable energy future," *Clean Energy*, vol. 9, no. 1, pp. 52–88, 2025, doi: 10.1093/ce/zkae112.
[4] T. Li *et al.*, "Dual-fuel dual-direct injection: an efficient and clean combustion technology for diesel engines," *Journal of the Energy Institute*, vol. 119, 2025, doi: 10.1016/j.joei.2025.102006.
[5] N. Saravanan, G. Nagarajan, K. M. Kalaiselvan, and C. Dhanasekaran, "An experimental investigation on hydrogen as a dual fuel for diesel engine system with exhaust gas recirculation technique," *Renewable Energy*, vol. 33, no. 3, pp. 422–427, 2008, doi: 10.1016/j.renene.2007.03.015.
[6] E. Dimitrov, M. Peychev, and A. Tashev, "Study of the hydrogen influence on the combustion parameters of diesel engine," *International Journal of Hydrogen Energy*, vol. 123, pp. 219–230, 2025, doi: 10.1016/j.ijhydene.2025.02.114.
[7] T. Xu, M. Wei, Z. Li, Q. Ji, P. Sun, and J. Liu, "Influence of pilot injection strategy on in-cylinder combustion, emissions and energy efficiency of hydrogen/diesel dual-fuel engine at low load," *Fuel*, vol. 399, 2025, doi: 10.1016/j.fuel.2025.135614.
[8] S. Das and B. Das, "Effect of injection parameters on the hydrogen enriched dual-fuel CRDI diesel engine," *Energy Sources, Part A: Recovery, Utilization and Environmental Effects*, vol. 45, no. 4, pp. 10176–10199, 2023, doi: 10.1080/15567036.2023.2240256.
[9] N. S. Kadhim, S. M. Adhas, E. Al-Mahdawi, and T. Milton, "Advances in hydrogen-diesel dual fuel engine technology: a systematic review of emissions and performance characteristics," *SSRG International Journal of Mechanical Engineering*, vol. 12, no. 3, pp. 61–70, 2025, doi: 10.14445/23488360/IJME-V12I3P105.
[10] X. Liu, S. Liu, L. Shen, Y. Bi, and L. Duan, "Study on the effects of the hydrogen substitution rate on the performance of a hydrogen–diesel dual-fuel engine under different loads," *Energies*, vol. 16, no. 16, 2023, doi: 10.3390/en16165971.
[11] M. U. S. Akhtar, F. Asfand, M. I. Khan, R. Mishra, and A. D. Ball, "Performance and emissions characteristics of hydrogen-diesel dual-fuel combustion for heavy-duty engines," *International Journal of Hydrogen Energy*, vol. 143, pp. 454–467, 2025, doi: 10.1016/j.ijhydene.2025.01.246.
[12] H. Mehnatkesh, D. Gordon, and C. R. Koch, "Dynamic emission analysis of a hydrogen/diesel dual-fuel engine using clustering method," *International Journal of Hydrogen Energy*, vol. 136, pp. 371–382, 2025, doi: 10.1016/j.ijhydene.2025.04.385.
[13] A. Ashok, S. K. Gugulothu, R. V. Reddy, and H. Ravi, "Box-behnken response surface methodology based multi-objective optimization on reactivity controlled compression ignition engine characteristics powered with ternary fuel," *Journal of Energy Resources Technology, Transactions of the ASME*, vol. 144, no. 12, 2022, doi: 10.1115/1.4054534.
[14] V. P. Chaudhary, M. K. Singh, and D. B. Lata, "Optimization of performance and emission parameters of hydrogen enriched dual fuel diesel engine using response surface methodology," *International Journal of Hydrogen Energy*, vol. 79, pp. 1100–1112, 2024, doi: 10.1016/j.ijhydene.2024.07.087.
[15] C. Tiwari, G. Dwivedi, and T. N. Verma, "Exploring the performance and emission characteristics of a dual fuel CI engine using microalgae biodiesel and diesel blend: a machine learning approach using ANN and response surface methodology," *Environment, Development and Sustainability*, vol. 27, no. 9, pp. 22877–22903, 2025, doi: 10.1007/s10668-024-05362-2.
[16] L. Breiman, "Random forests," *Machine Learning*, vol. 45, no. 1, pp. 5–32, Oct. 2001, doi: 10.1023/A:1010933404324.
[17] V. Kovalnogov, R. Fedorov, V. Klyachkin, D. Generalov, Y. Kuvayskova, and S. Busygin, "Applying the random forest method to improve burner efficiency," *Mathematics*, vol. 10, no. 12, 2022, doi: 10.3390/math10122143.
[18] J. Liu, Q. Huang, C. Ulishney, and C. E. Dumitrescu, "Comparison of random forest and neural network in modeling the performance and emissions of a natural gas spark ignition engine," *Journal of Energy Resources Technology, Transactions of the ASME*, vol. 144, no. 3, 2022, doi: 10.1115/1.4053301.
[19] D. Wintergoller, A. Dafis, and H. Rottengruber, "Analysis of hydrogen combustion in a commercial vehicle engine using 1D Simulation and Subsequent CFD Simulation," *SAE Technical Papers*, 2023, doi: 10.4271/2023-01-1642.
[20] S. Tüchler and P. Dimitriou, "On the capabilities and limitations of predictive, multi-zone combustion models for hydrogen-diesel dual fuel operation," *International Journal of Hydrogen Energy*, vol. 44, no. 33, pp. 18517–18531, 2019, doi: 10.1016/j.ijhydene.2019.05.172.
[21] J. B. Heywood, *Internal Combustion Engine Fundamentals*. New York, USA, 2018, doi: 10.1201/9780203734858-6.
[22] N. Saravanan, G. Nagarajan, C. Dhanasekaran, and K. M. Kalaiselvan, "Experimental investigation of hydrogen port fuel injection in DI diesel engine," *International Journal of Hydrogen Energy*, vol. 32, no. 16, pp. 4071–4080, 2007, doi: 10.1016/j.ijhydene.2007.03.036.
[23] X. Liu, A. Srna, H. L. Yip, S. Kook, Q. N. Chan, and E. R. Hawkes, "Comparison of hydrogen port injection and direct injection (DI) in a single-cylinder dual-fuel diesel engine," in *22nd Australasian Fluid Mechanics Conference, AFMC 2020*, 2020, doi: 10.14264/a1cd1dc.
[24] S. Javed, Y. V. V. Satyanarayana Murthy, M. R. S. Satyanarayana, R. Rajeswara Reddy, and K. Rajagopal, "Effect of a zinc oxide nanoparticle fuel additive on the emission reduction of a hydrogen dual-fuelled engine with jatropha methyl ester biodiesel blends," *Journal of Cleaner Production*, vol. 137, pp. 490–506, 2016, doi: 10.1016/j.jclepro.2016.07.125.
[25] L. Breiman, *Bagging predictors*, vol. 24, no. 2. 1996, doi: 10.1023/A:1018054314350.
[26] A. Srinivaas, N. R. Sakthivel, and B. B. Nair, "Machine learning approaches for fault detection in internal combustion engines: a review and experimental investigation," *Informatics*, vol. 12, no. 1, 2025, doi: 10.3390/informatics12010025.
[27] K. Karunamurthy, M. M. Feroskhan, G. Suganya, and I. Saleel, "Prediction and optimization of performance and emission characteristics of a dual fuel engine using machine learning," *International Journal for Simulation and Multidisciplinary Design Optimization*, vol. 13, 2022, doi: 10.1051/smdo/2022002.
[28] K. S. Varde and G. A. Frame, "Hydrogen aspiration in a direct injection type diesel engine-its effects on smoke and other engine performance parameters," *International Journal of Hydrogen Energy*, vol. 8, no. 7, pp. 549–555, 1983, doi: 10.1016/0360-3199(83)90007-1.
[29] V. S. Yadav, S. L. Soni, and D. Sharma, "Engine performance of optimized hydrogen-fueled direct injection engine," *Energy*, vol. 65, pp. 116–122, 2014, doi: 10.1016/j.energy.2013.12.007.
[30] H. P. Rajagopalan, R. Cole, D. Wu, B. Emerson, and T. Lieuwen, "Turbulent burning velocity of high hydrogen flames," *Proceedings of the ASME Turbo Expo*, vol. 3A-2024, 2024, doi: 10.1115/GT2024-121349.
[31] J. M. Rueda-Vázquez, J. Serrano, S. Pinzi, F. J. Jiménez-Espadafor, and M. P. Dorado, "A review of the use of hydrogen in compression ignition engines with dual-fuel technology and techniques for reducing NOx emissions," *Sustainability (Switzerland)*, vol. 16, no. 8, 2024, doi: 10.3390/su16083462.
[32] H. Ge, A. H. Bakir, and P. Zhao, "Knock mitigation and power enhancement of hydrogen spark-ignition engine through ammonia blending," *Machines*, vol. 11, no. 6, 2023, doi: 10.3390/machines11060651.
[33] A. Kumar, C. Bhushan Kumar, and D. B. Lata, "Effect of hydrogen enrichment on exhaust gas temperature and emission of a dual fuel diesel engine," *Materials Today: Proceedings*, vol. 72, pp. 631–635, 2023, doi: 10.1016/j.matpr.2022.08.232.

[34] M. Senthil Kumar, A. Ramesh, and B. Nagalingam, "Use of hydrogen to enhance the performance of a vegetable oil fuelled compression ignition engine," *International Journal of Hydrogen Energy*, vol. 28, no. 10, pp. 1143–1154, 2003, doi: 10.1016/S0360-3199(02)00234-3.
[35] T. Miyamoto, H. Hasegawa, M. Mikami, N. Kojima, H. Kabashima, and Y. Urata, "Effect of hydrogen addition to intake gas on combustion and exhaust emission characteristics of a diesel engine," *International Journal of Hydrogen Energy*, vol. 36, no. 20, pp. 13138–13149, 2011, doi: 10.1016/j.ijhydene.2011.06.144.
[36] A. M. L. M. Wagemakers and C. A. J. Leermakers, "Review on the effects of dual-fuel operation, using diesel and gaseous fuels, on emissions and performance," *SAE Technical Papers*, 2012, doi: 10.4271/2012-01-0869.
[37] R. Farzam *et al.*, "Performance and emissions characteristics of hydrogen-diesel heavy-duty engines: the influence of engine control parameters," *International Journal of Hydrogen Energy*, vol. 109, pp. 1325–1340, 2025, doi: 10.1016/j.ijhydene.2025.02.135.
[38] H. W. Wu and Z. Y. Wu, "Investigation on combustion characteristics and emissions of diesel/hydrogen mixtures by using energy-share method in a diesel engine," *Applied Thermal Engineering*, vol. 42, pp. 154–162, 2012, doi: 10.1016/j.applthermaleng.2012.03.004.
[39] V. E. Geo, G. Nagarajan, and B. Nagalingam, "Studies on dual fuel operation of rubber seed oil and its bio-diesel with hydrogen as the inducted fuel," *International Journal of Hydrogen Energy*, vol. 33, no. 21, pp. 6357–6367, 2008, doi: 10.1016/j.ijhydene.2008.06.021.
[40] H. Köse and M. Ciniviz, "An experimental investigation of effect on diesel engine performance and exhaust emissions of addition at dual fuel mode of hydrogen," *Fuel Processing Technology*, vol. 114, pp. 26–34, Oct. 2013, doi: 10.1016/j.fuproc.2013.03.023.
[41] M. T. Chaichan, "The impact of equivalence ratio on performance and emissions of a hydrogen-diesel dual fuel engine with cooled exhaust gas recirculation," *International Journal of Scientific & Engineering Research*, vol. 6, no. 6, pp. 938–945, 2015, [Online]. Available: http://www.ijser.org.
[42] P. Dimitriou, M. Kumar, T. Tsujimura, and Y. Suzuki, "Combustion and emission characteristics of a hydrogen-diesel dual-fuel engine," *International Journal of Hydrogen Energy*, vol. 43, no. 29, pp. 13605–13617, Jul. 2018, doi: 10.1016/j.ijhydene.2018.05.062.
[43] A. E. Dhole, R. B. Yarasu, D. B. Lata, and A. Priyam, "Effect on performance and emissions of a dual fuel diesel engine using hydrogen and producer gas as secondary fuels," *International Journal of Hydrogen Energy*, vol. 39, no. 15, pp. 8087–8097, May 2014, doi: 10.1016/j.ijhydene.2014.03.085.
[44] E. Tian, G. Lv, and Z. Li, "Evaluation of emission of the hydrogen-enriched diesel engine through machine learning," *Energy*, vol. 307, p. 132303, Oct. 2024, doi: 10.1016/j.energy.2024.132303.
[45] S. C. de L. Nogueira, S. H. Och, L. M. Moura, E. Domingues, L. dos S. Coelho, and V. C. Mariani, "Prediction of the NOx and CO2 emissions from an experimental dual fuel engine using optimized random forest combined with feature engineering," *Energy*, vol. 280, 2023, doi: 10.1016/j.energy.2023.128066.
[46] A. A. M. Mohammedali, A. Albadwi, A. A. M. Omara, K. Ali, and M. I. H. Ali, "Machine learning prediction and evolutionary multi-objective optimization on performance and emissions of a syngas-diesel dual-fuel engine," *International Journal of Hydrogen Energy*, vol. 162, 2025, doi: 10.1016/j.ijhydene.2025.150781.
[47] B. Eren and İ. Cesur, "Comparative analysis of machine learning models for CO emission prediction in engine performance," *Sakarya University Journal of Computer and Information Sciences*, vol. 8, no. 1, pp. 1–11, 2025, doi: 10.35377/saucis...1564937.
[48] J. Liu, C. Ulishney, and C. E. Dumitrescu, "Random forest machine learning model for predicting combustion feedback information of a natural gas spark ignition engine," *Journal of Energy Resources Technology, Transactions of the ASME*, vol. 143, no. 1, 2021, doi: 10.1115/1.4047761.

BIOGRAPHIES OF AUTHORS

Jayagopal Narayanan is a research scholar in Indian Maritime University. Presently, he is the general manager at Kirloskar Oil Engine, Development Division, Pune. His area of research is engine simulation, modelling, and simulation. He can be contacted at email: jayagopalnarayanan@gmail.com.

Y. V. V. Satyanarayana Murthy presently working as an associate professor in Indian Maritime University, research supervisor, and practising engineer. His research area includes large bore engines, fuels, marine machinery systems, safety, and vibration control. He can be contacted at email: yvvsnmurthy@imu.ac.in.

Sandeep Kumar is a research scholar in Indian Maritime University, ex chief marine engineer, and CEO. His area of research is computational fluid dynamics and hydraulic systems. He can be contacted at email: sandeepkumar2311@gmail.com.

Talari Surendra is professor of mechanical engineering at GITAM (Deemed to be University), Visakhapatnam, India. His expertise is in modelling and simulation of mechanical systems, noise, and vibration control. He can be contacted at email: stalari@gitam.edu.

Ram Mohan Rao Madaka is assistant professor of mechanical engineering at GITAM (Deemed to be University), Visakhapatnam, India. His expertise is in modelling and simulation of mechanical systems, noise, and vibration control. He can be contacted at email: mrammohanrao@gmail.com.